Correlated Photon Pair Source for Telecommunications

Kenneth Ho Jun Hao

National University of Singapore

Department of Physics

A thesis submitted for the degree of

B.Sc. (Hons)

AY 2017/2018

Acknowledgements

Working on this project for the past year has been an unforgettable journey and the skills that I have picked up from it will stay with me for the rest of my life. I would like to thank Professor Alexander Ling and Dr. James Grieve for allowing me to take on this challenge and for the guidance they have provided me throughout this journey. My thanks also to Soe Moe Thar and Lincoln Lee for the ever interesting conversations from physics to any other possible topic under the sun and also for assisting me in anything related to electronics and computing. I would also like to thank everyone from the Singtel Corp Lab Theme 4 and from the Quantum Optics group for all the help and feedback that you all have given me, without which I would not have been able to accomplish what I have. Finally, my thanks goes out to my friends and family and especially my girlfriend, Jia Ying, without whom, would have made this journey so much more difficult.

Abstract

This project aims to investigate and design an optical set-up to produce correlated photon pairs for use in quantum applications. In this thesis, I look at the designing and testing of a correlated photon pair source that produces correlated photon pairs through Spontaneous Parameteric Down Conversion (SPDC) with wavelengths in the telecommunication O-band. These correlated photon pairs would eventually be used to perform clock synchronisation over long distances of optical fibers. This thesis will also cover the measures taken to mitigate the effects of chromatic dispersion in optical fibers which would hinder the accuracy of the clock synchronisation experiment. Finally, I will cover the designing of a compact version of the source by testing two different configurations. After the testing, we shall look at the capabilities of the compact source and look at its possible applications.

Contents

List of Figures

List of Tables

Chapter 1

Introduction

1.1 Background

As we enter the age of information, where most of the information around us is digitised, the demand for a secure form of communication has increased greatly. In order to meet this demand, much research has been done into parametric down conversion to produce correlated and entangled photon pairs as a way to encrypt data so as to ensure that we have our privacy[4].

Correlated photon pairs are photons that are strongly correlated in time, energy and polarisation. These correlations can be used as a form of secure information carrier which can be used in various quantum applications. Some quantum applications of correlated photons pairs are in clock synchronisation [5] and more importantly in Quantum Key Distribution (QKD) where these photons can be used to encrypt our data so that we can ensure the privacy of our digital communications [6][7][8][9]. This is especially important as classical forms of cryptography would not be secure with the expected advancements in quantum computing. Hence, QKD would be one of the ways that we can ensure that our data would be secure and private in a world with quantum computing. There are two main methods of QKD currently used, they are the BB84 protocol[9] and the use of entanglement based QKD[10]. The BB84 protocol is now commercially available but requires a truly random number generator to work efficiently. Entangled based QKD however, does not require this as the randomness is built into the photons themselves. Furthermore, another advantage that entanglement based QKD has over BB84, is that it allows of a central provider for the entangled photons unlike BB84 where each user requires both a source and detector.

With the research into these applications, a minor problem arises. How do these photons get from one place to another? In recent years, much development has been done in transmitting these photons through free space which can be seen in various satellite QKD systems [11][12]. Another possible mode for transmission is through optical fibers which is much more applicable in an urban setting. However, the problem with optical fibers is that it would be difficult to implement these applications commercially due to the fibers needing to be directly linked to each location and to do so would require the installation of new underground fiber links which would be very expensive or alternatively, to use currently available dark fibers. The fibers are optimised for certain wavelengths in the telecommunications band and most research into the production of photon pairs in the telecommunication bands has been focused on the telecommunications C-band (wavelengths ≈1550nm) and very little has been done on the O-band (wavelengths ≈1310nm). The O-band is preferred as the detector efficiency for photons in this region is slightly higher than the C-band [13]. Hence, this thesis looks at the production of correlated photons in the O-band in order to eventually produce a source that can be used for quantum applications over optical fibers.

1.2 Objectives

In this project, I aim to firstly, build a correlated photon pair source that produces correlated photon pairs with a center wavelength in the telecommunication O-band which can be used in optical fibers. Secondly, test the source and maximise the coincidence pair rates to optimise its efficiency. Finally, I design and test a compact baseplate prototype of the source so that future tests can be performed in the field using currently buried fibers around Singapore.

1.3 Motivations

This project is the precursor to an entangled photon pair source that will produce photons at the same wavelengths. This source however is also important as it is part of a collaboration between the Center of Quantum Technologies (CQT) in NUS and Singapore Telecommunications (Singtel) to build a correlated photon pair source to perform clock synchronisation over buried optical fibers around Singapore.

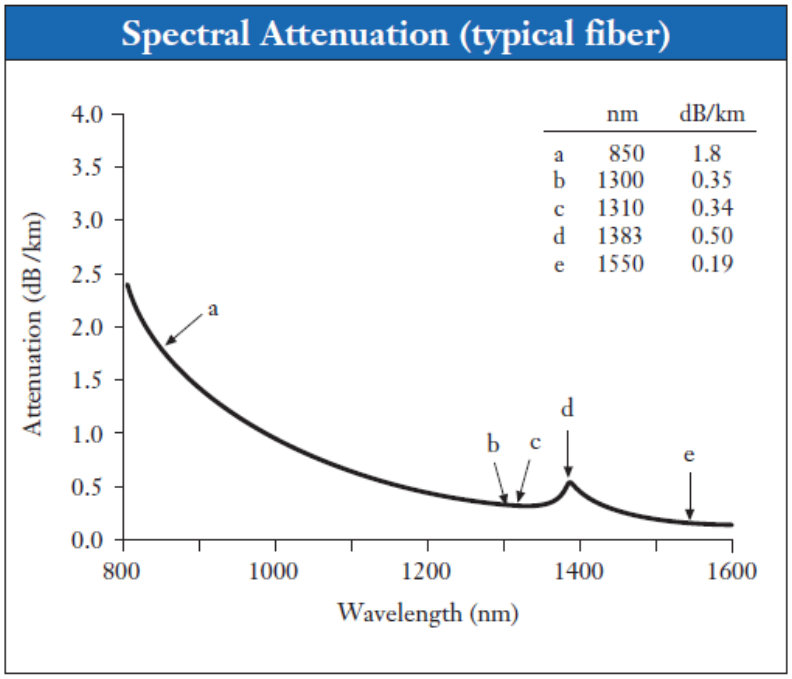

Figure 1.1: Attenuation of light of different wavelengths through an optical fiber Taken from SMF-28 Datasheet [1]

Correlated and entangled photon pair sources are a well researched topic in the field of Quantum Optics. However, most of these research have involved the transmission of the photon pairs over free space and hence, the wavelengths of the generated photons are typically in the range of 700 to 800nm. These wavelengths are not able to propagate through optical fibers efficiently as they would experience massive losses due to attenuation as seen in Figure 1.1 taken from the datasheet of a standard SMF-28 optical fiber (Corning)[1].

Therefore, in this project, I investigate the production of correlated photon pairs in the telecommunications O-band which can propagate through fibers with attenuation losses of 0.4dB/km. With the knowledge gained from the experiments, I then start to design and prototype a compact baseplate version of the pair source that can sit in a server rack to produce correlated photon pairs that would eventually be used to perform clock synchronisation, where the main idea of the experiment is to use correlated photons to synchronise two clocks at different locations using the fact that the photons are produced at the same time and have a strong timing correlation.[5]

Chapter 2

Theory

2.1 Spontaneous Parametric Down Conversion

2.1.1 The Nonlinear Susceptibility

Spontaneous Parametric Down Conversion (SPDC), is in brief the process where a higher energy photon splits into two lower energy photons through the interaction with a nonlinear optical material. It is a three-wave mixing process that makes use of the second order nonlinearity of a nonlinear optical material. I begin by looking at the polarisation of a nonlinear material. In a normal linear medium, the polarisation is given by

$$\mathbf{P}(t) = \epsilon_0 \chi^{(1)} \mathbf{E} \tag{2.1}$$

where ϵ_0 is the permittivity of free space and $\chi^{(1)}$ is the linear susceptibility of the material.

For a general nonlinear material, the equation 2.1 can be expanded as a power series giving

$$\mathbf{P}(t) = \epsilon_0(\chi^{(1)}\mathbf{E} + \chi^{(2)}\mathbf{E}^2 + \chi^{(3)}\mathbf{E}^3 + ...) \tag{2.2}$$

where $\chi^{(2)}$ and $\chi^{(3)}$ are the second and third order nonlinear optical susceptibility of the material. [14]

For SPDC, since it a second order process [15], I would focus on the $\chi^{(2)}$ nonlinearity tensor. The equation 2.2 can be broken down into two components. The linear component is the same as equation 2.1 while for a second order process, the nonlinear component is

$$\mathbf{P}^{NL}(t) = \epsilon_0 \chi^{(2)} \mathbf{E}^2 \tag{2.3}$$

The nonlinear component connects the incoming electric field with two outgoing electric fields. Assuming the electric field is in the form $\mathbf{E} = A\cos\omega t$, the nonlinear component would now be

$$\mathbf{P}^{NL}(t) = \frac{1}{2}\epsilon_0\chi^{(2)}A^2(1+\cos 2\omega t) \tag{2.4}$$

From equation 2.4, we can see that it is possible in a second order nonlinear medium to produce electric fields with a frequency that is double the original field. This is known as second harmonic generation. [15]

SPDC is essentially the opposite of second harmonic generation where instead of 2 photons of lower frequency interact with the medium to produce a higher frequency photon, a high frequency photon, also called the pump photon, interacts with the medium to generate 2 lower frequency photons known as the signal and idler. It is these signal and idler photons produced from down-conversion that shall be the main focus of this thesis.

2.1.2 Conservation Laws & Phase Matching

The signal and idler photons obey the laws of conservation of energy and momentum. In terms of frequency, equation showing the conservation of energy is

$$\omega_p = \omega_s + \omega_i \tag{2.5}$$

where the subscripts p, s and i stands for the pump, signal and idler respectively. In terms of wavelength, the same equation can be rewritten into

$$\frac{1}{\lambda_p} = \frac{1}{\lambda_s} + \frac{1}{\lambda_i} \tag{2.6}$$

For SPDC to occur, another condition known as the phase matching condition or the conservation of momentum has to be fulfilled.

$$\overrightarrow{k_p} = \overrightarrow{k_s} + \overrightarrow{k_i} \tag{2.7}$$

Where the wavevectors $\overrightarrow{k_j} = \frac{n_j\omega_j}{c}$ for j = p, s, i.

Due to chromatic dispersion, which is when the refractive index depends on the frequency of the photon, the phase matching condition may not be met exactly. Hence, in order for this condition to be fulfilled, only certain materials with a suitable

refractive index can be used. Usually, the medium used for phase matching are anisotropic, birefringent crystals, whose refractive indices can be tuned by either changing temperature or the angle between the propagation direction of the pump and the crystal optical axis [16].

This process is known as phase matching. The first method of phase matching by tuning the angle between the pump and the optical axis is called critical phase matching (CPM) [17][7]. The other method to achieve phase matching is to adjust the temperature of the crystal which would affect the refractive index of the birefringent crystal [17][18]. This method is known as non-critical phase matching. These methods effectively link the signal and idler wavelengths and polarisation to that of the pump's.

To distinguish between the cases when the down-converted photons have parallel or orthogonal polarisations to each other and to the pump, they are labelled as Type-0, Type-I or Type-II SPDC. When the polarisations of the pump, signal and idler are the same, this is known as Type-0 SPDC. If the polarisation of the signal and idler are orthogonal to the pump, it is called Type-I or Type-II SPDC if the signal and idler are parallel or orthogonal to each other respectively. In this thesis, I shall mainly look at Type-0 and Type-II SPDC.

Phase matching is an important condition to achieve as it is directly related to the efficiency of the down conversion process. If the condition is not satisfied, the amplitude contributions from different parts of the crystal would not interfere constructively as the pump and the signal and idler would be out of phase after every one coherence length causing the amplitude to oscillate. Only when this condition is satisfied will the amplitudes add up constructively and allow for efficient photon generation.

2.2 Quasi-Phase Matching

Besides the two methods outlined in the previous section, there exists another method called Quasi-Phase Matching (QPM) that can be used to fulfil the phase matching condition [2] [19]. Quasi-Phase Matching is a technique whereby a specially engineered crystal is used to satisfy the phase matching condition [20]. This technique was first suggested by Armstrong et al.[21] as well as Franken and Ward[22], as a method to achieve phase matching by using a a nonlinear crystal that has periodically alternating optical axes [23]. The flipping of the optical axes would cause the nonlinear coefficient to change its sign every one coherence length [8] and the amplitude of the down converted field would increase as seen in Figure 2.1

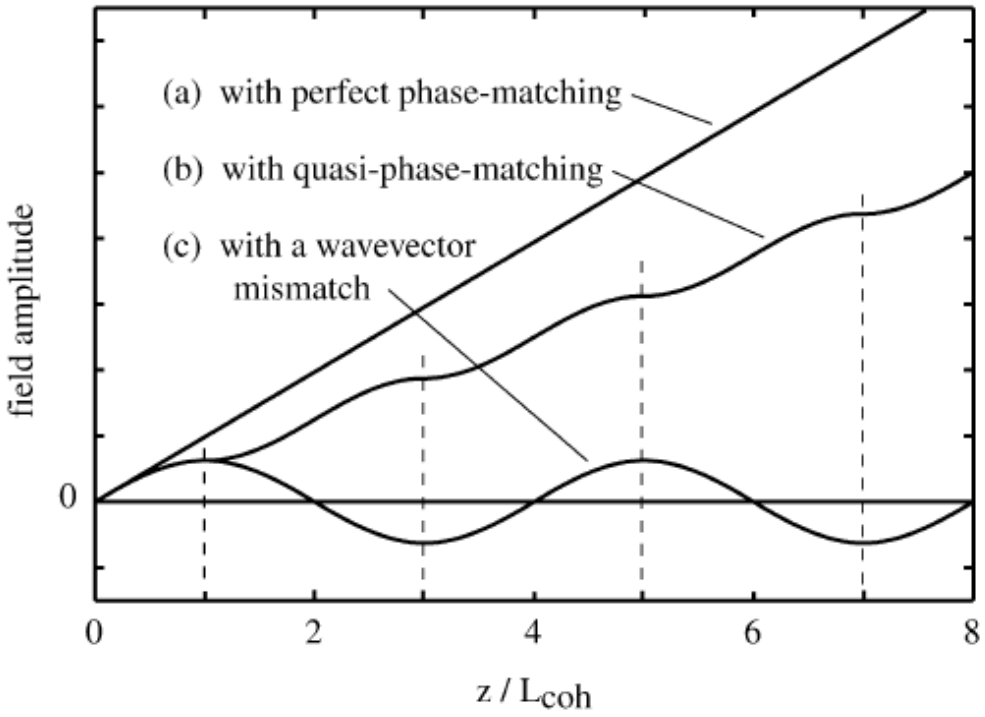

Figure 2.1: Comparing the Amplitude of the down converted field for three different phase matching conditions. Taken from [2]

From Figure 2.1, it is clear that in QPM, the efficiency of the photon conversion would be lower than when there is perfect phase matching. However, in general, it is much easier to achieve phase matching using QPM compared to the traditional methods outlined previously as it is not as sensitive to changes in the angle between the pump and the optical axis of the crystal[22]. Furthermore, QPM would also allow us to use larger nonlinear coefficients that may not be available for use when using normal phase matching methods [7]. This is especially important as in Type-0 SPDC, where the pump, signal and idler are all in the same polarisation, CPM cannot be used as all the photons see the same optical axis [2].

To obtain QPM, I use a periodically poled crystal where the nonlinear crystal has its optical axis inverted periodically. The poling period Λ of the crystal effectively adds an additional k vector into equation 2.7.

$$\overrightarrow{k_p}(n_p(\omega_p, T)) = \overrightarrow{k_s}(n_s(\omega_s, T)) + \overrightarrow{k_i}(n_i(\omega_i, T)) + \overrightarrow{K}(T) \tag{2.8}$$

where $\overrightarrow{K} = \frac{2\pi}{\Lambda(T)}$ is the additional k vector added to the equation due to the periodic poling. This additional wavevector would help to satisfy the phase matching condition

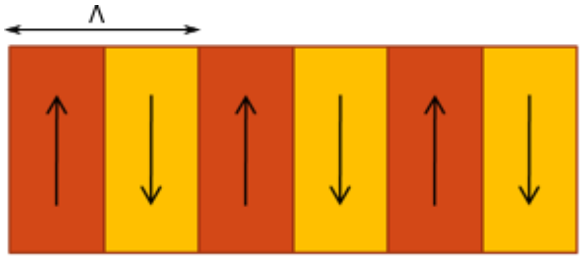

Figure 2.2: Periodic poling of a nonlinear optical crystal with poling period Λ

by specially engineering the crystal to have a specific poling period Λ. This poling period is also sensitive to temperature, hence, it is possible to temperature tune the crystal to allow phase matching for various pump wavelengths [8]. In this thesis, the main phase matching method used would be QPM combined with temperature tuning of the crystal to satisfy the phase matching condition.

2.3 Spectrum of Down Converted Photons

Even when using QPM and temperature tuning, there would still be a phase mismatch since it is difficult to obtain perfect phase matching in reality. This phase mismatch is given by

$$\Delta \overrightarrow{k} = \overrightarrow{k_p}(n_p(\omega_p, T)) - \overrightarrow{k_s}(n_s(\omega_s, T)) - \overrightarrow{k_i}(n_i(\omega_i, T)) - \overrightarrow{K}(T) \tag{2.9}$$

The average photon flux generated by SPDC is given by

$$\langle n_s \rangle = \langle n_i \rangle = |\kappa a_p|^2 \tag{2.10}$$

where $|a_p|^2$ is directly proportional to the intensity of the pump, and $|\kappa|^2$ is related to the efficiency of conversion of the pump to the signal and idler. The κ parameter is directly proportional to the sinc function that involves the phase mismatch $\mathbf{\Delta k}$

$$\kappa \propto L d_{eff} sinc(\frac{\Delta k L}{2}) \tag{2.11}$$

where L is the length of the crystal and d_{eff} is the effective nonlinear coefficient.[24] From the equation, the spectrum of the down converted photons would be proportional to a sinc function. This allows us to predict the output spectra for a given set of pump wavelengths and poling periods. It also allows us to simulate the appropriate crystal temperature in order to obtain proper quasi-phase matching.

Chapter 3

Crystal Characterisation

3.1 Experimental Objectives

In this experiment, I aim to test the efficiency for various configurations for the correlated photon pair source so as to choose the best setup for the baseplate version of the source. I tested and characterise two different types of crystals, Type-II Periodically Poled Lithium Niobate (PPLN) and Type-0 Periodically Poled Potassium Titanyl-Phosphate (PPKTP).

3.2 Setup

The setup for the experiment is shown in Figure 3.1.

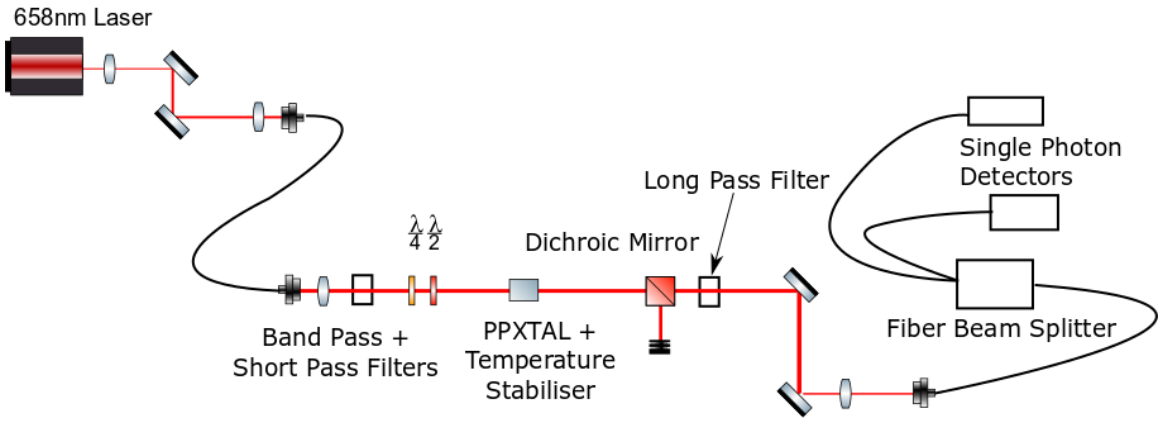

Figure 3.1: Diagram of Experimental Setup

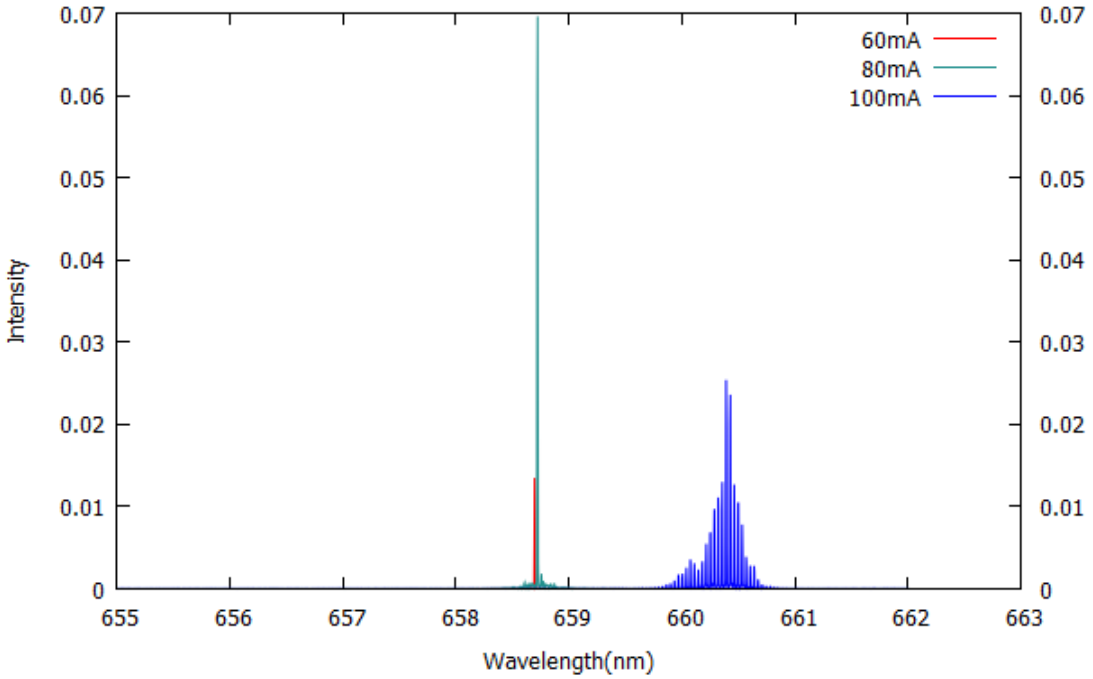

Figure 3.2: Laser Spectrum of Ondax SureLock 658nm X7575 Laser Diode

The pump laser used is an Volumetric Holograpic Grating (VHG) stabilised 658nm Wavelength Laser Diode (Ondax SureLock 658nm) that produces photons with a wavelength of 658nm. The spectrum of the laser output is shown in Figure 3.2.

The laser is first coupled into a single mode fiber using mirrors and lenses to filter off unwanted fluorescence coming from the laser diode. The pump is then launched into the main part of the setup with the crystal and passed through some short pass and band pass filters to remove any leftover fluorescence from the beam. The polarisation of the beam is then adjusted using a Quarter Wave Plate (QWP) and Half Wave Plate (HWP). This is necessary as when the beam propagates through the fiber, I would expect the polarisation state to be in a elliptical state due to birefringence in the fiber. The QWP would allow us to change the polarisation state back to a linear state while the HWP would allow me to rotate the state to any desired linear polarisation state. The beam is then focused into the crystal which is temperature stabilised using a Peltier Thermoelectric Cooler (TEC). The signal and idler photons would be produced in the crystal through SPDC. The pump is removed after the crystal using a dichroic mirror and long pass filters so that only the down-converted photons can pass through. The down-converted photons are then collected and coupled into a single mode fiber beam splitter which splits the signal and idler into different arms. The

photons are then detected by two InGaAs (Indium-Gallium-Arsenide) single photon detector (ID220, ID Quantique).

3.3 Beam Parameters

The pump is focused into the crystal using a lens placed before the band pass and short pass filters. By changing the lens and the distance of the lens to the crystal, I am able to adjust the Full Width Half Maximum (FWHM) of the pump at the centre of the crystal. According to Bennink (2010)[25] and Dixon (2014)[26], the optimal FWHM of the pump and collection at the center of the crystal is ≈112nm and ≈57nm respectively. To achieve this, I calculated the approximate focal length lens and distances between the lens and the center of the crystal using the propagation of a Gaussian wave with an ABCD matrix. The calculations are shown in the Appendix.

From the calculations, I selected and tested various combinations of lenses and distances. The FWHM of each combination is measured using a CMOS camera (Chameleon III,PointGrey) for the pump. The collection FWHM is measured by using a 1310nm laser pumped at the collection end of the setup. This is measured using a InGaAs camera (Xenics). The spots for both the pump and the collection and the fit of the spot is shown in the Figures 3.3 and 3.4.

The combinations chosen for the pump and the collection is shown in Table 3.1

	Lens Focal Length (mm)	Distance of Lens to Center of Crystal (cm)
Pump	11.0	37.50
Collection	18.4	36.25

Table 3.1: Focal length and Distance selected for experiment

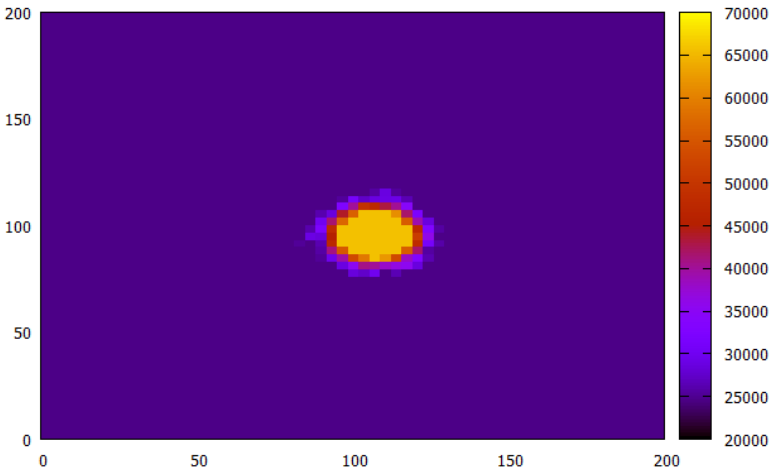

(a) Image of Pump Spot taken from CMOS camera. x and y axes are in μm

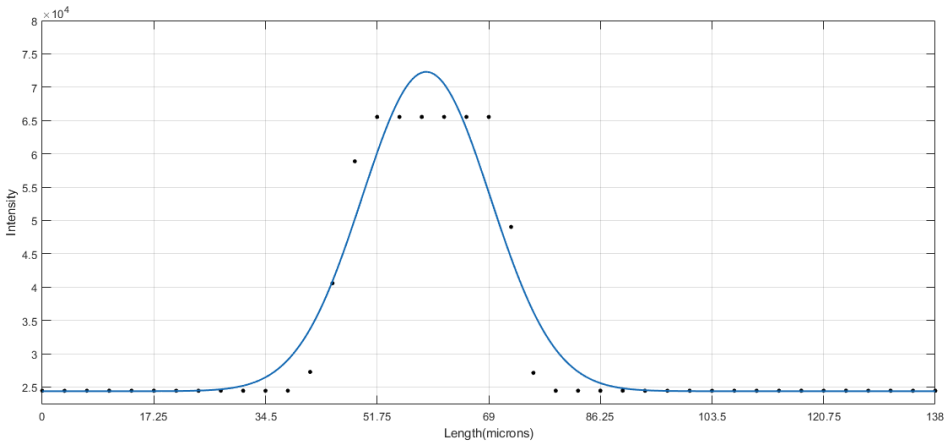

(b) Gaussian Fit of the Pump Spot

Figure 3.3: Pump Spot and its Gaussian fit

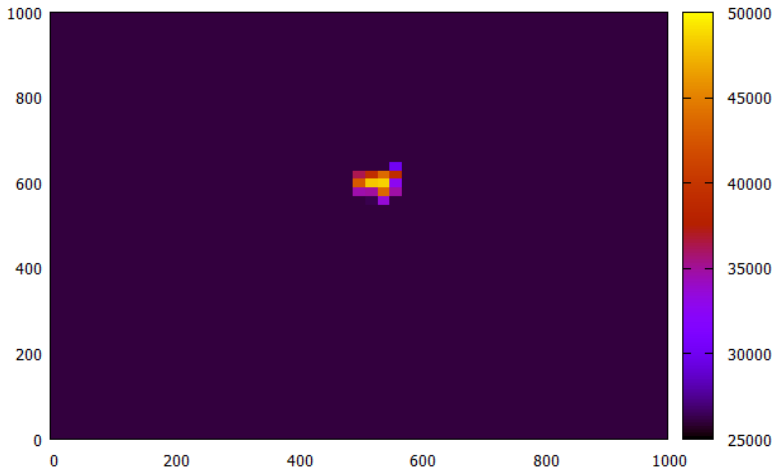

(a) Image of Collection Spot taken from InGaAs camera. x and y axes are in μm

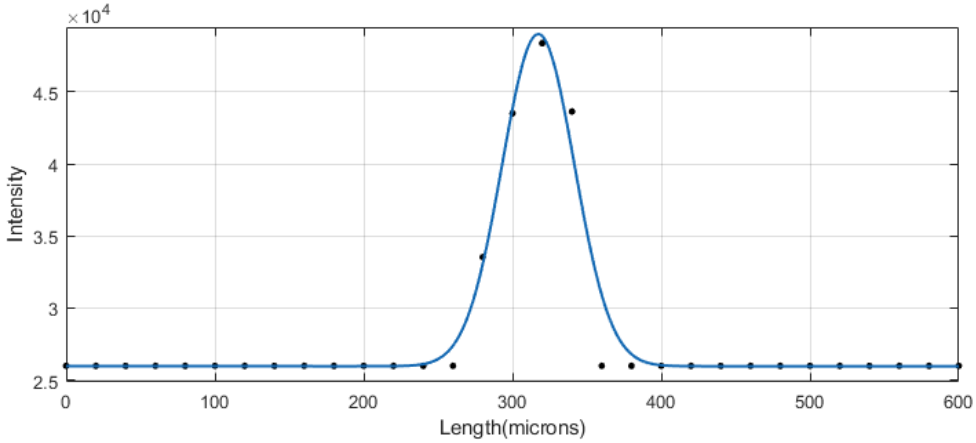

(b) Gaussian Fit of the Collection Spot

Figure 3.4: Collection Spot and its Gaussian fit

3.4 Type-II Periodically Poled Lithium Niobate

I first start the experiment by using a Type-II Periodically Poled Lithium Niobate (PPLN) (HC Photonics) as the crystal. The crystal has a poling period of 6.63μm. For Type-II-SPDC in PPLN, the output is dependant on the d_{31} nonlinear coefficient which has a magnitude of ≈4.4 pm/V[27][28].

3.4.1 Counting Singles and Coincidences

The crystal is temperature stabilised at 24°C using a Peltier TEC. The collected photons are split into two arms using a 50:50 fiber beam splitter and are detected by

the InGaAs detectors which send the counts to a computer to plot the counts and the coincidences on a graph which is updated constantly. A coincidence is defined as an event when a photon is detected on each detector within a 3.6ns window.

3.4.2 Crystal Temperature Tuning

The crystal temperature has to be stabilised as thermal expansion can cause the poling period to change. Furthermore, a change in the temperature would also lead to a change in the refractive indices of the crystal which vary for different crystals. These changes would lower the brightness of the source as the phase matching condition would not be satisfied. Hence, it is important to find the temperature that the source would be the brightest and stabilise it effectively. The temperature of the crystal is stabilised by using a copper block that is attached to a Peltier TEC. This allows us to change the temperature and stabilise it by varying the current supplied to the TEC.

To find the optimal temperature, the source is first aligned until I obtain maximum coincidences. I then run the signal and idler photons into a spectrometer that allows me to view the spectrum of the SPDC photons. The spectrometer makes use of a blazed diffraction grating and an automated rotation stage to obtain the spectrum. The equation relating the angle of rotation and the wavelength of the photon is given by

$$\lambda = \frac{1}{n}(\sin\theta + \sin(\theta_{1st} + \theta)) \tag{3.1}$$

where n is the number of grooves per nm, θ_{1st} is the angle where the first order spot for 1310nm is detected and θ is the angle of rotation.

After running the signal and idler photons through the spectrometer at different temperatures, I obtain the plot shown in Figure 3.5. It should be noted that at this point of the experiment, I was not yet using the laser diode specified above. This spectrum was taken using a 658nm laser diode that showed some multimode characteristics (HL6501MG, Opnext).

From Figure 3.5, I can see that at 23.5°C, the peaks are the highest. Hence, the operating temperature for PPLN is set at 23.5°C. Figure 3.6 shows the spectrum taken again at 23.5°C after changing to the VHG stabilised laser diode (Ondax SureLock 658nm).

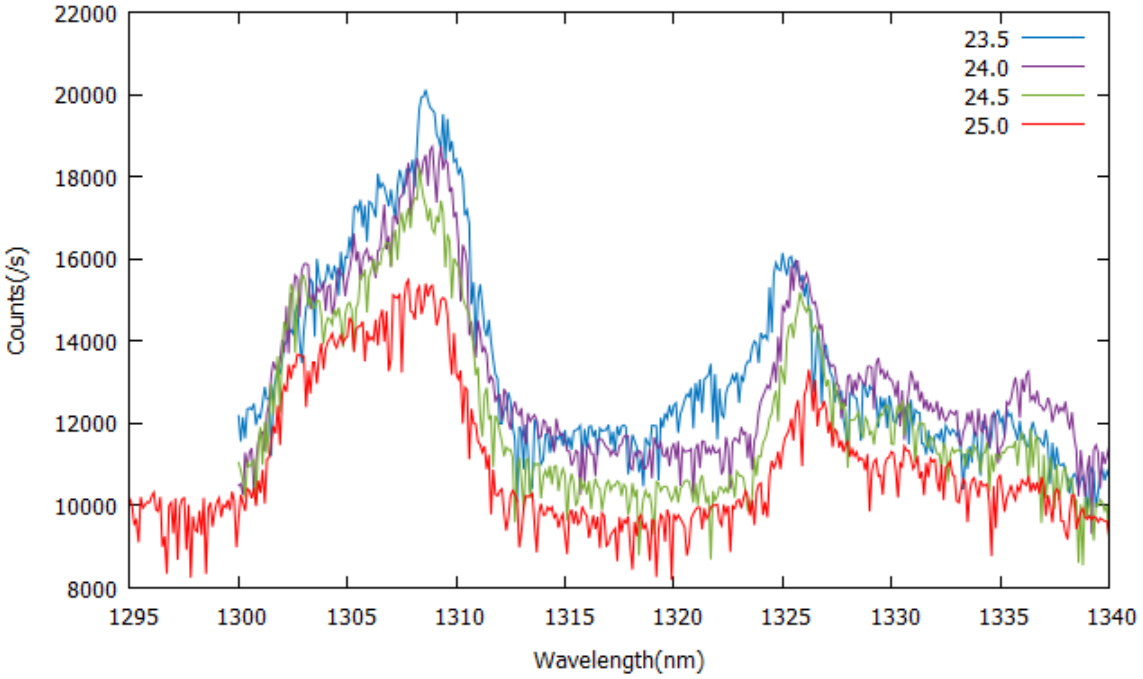

Figure 3.5: Spectrum of SPDC photons using PPLN at various temperatures using multimode laser diode

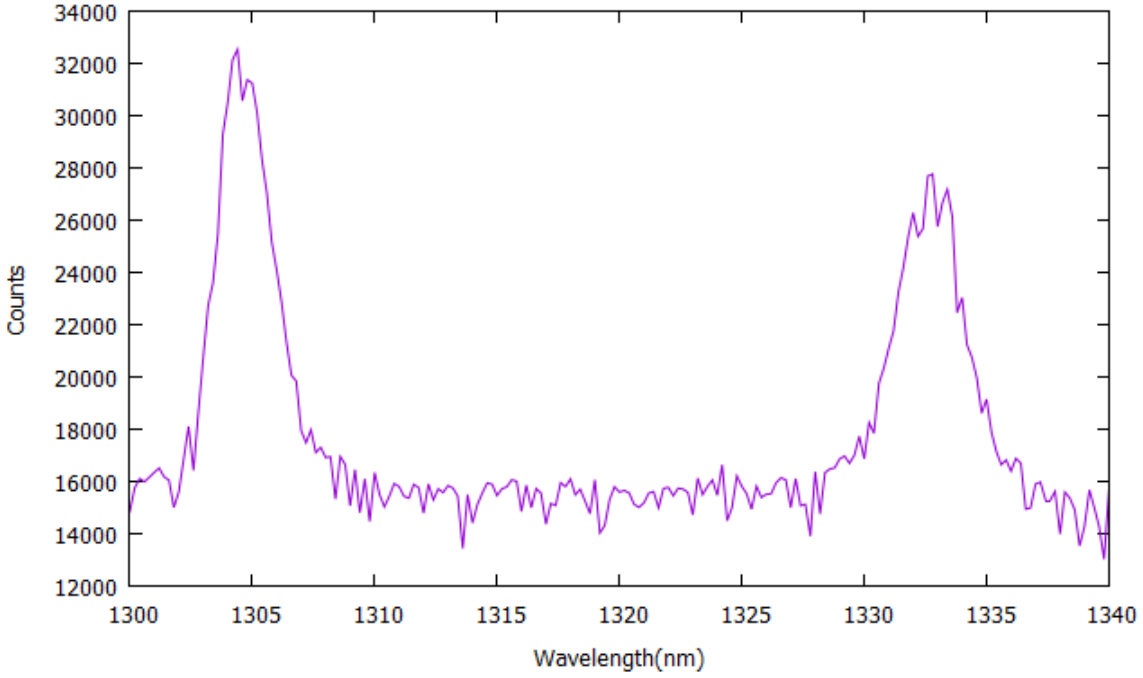

Figure 3.6: Spectrum of SPDC photons using PPLN at T=23.5°C using Ondax Laser Diode

3.4.3 Optimising Coincidence Rates

With the appropriate operating temperature found, I then started to further optimise the coincidence rates of the source by tuning the collection mirrors. At this time of the experiment, I obtained a dichroic fiber beam splitter centered at 1320nm that can efficiently split the signal and idler into both arms. This would effectively increase coincidences by a factor of two compared to using the 50:50 splitter where there is a 50% chance that both signal and idler photons enter the same arm and no coincidence is detected. After optimisation with the new beam splitter, the maximum coincidence rate observed is $\approx$ 300 pairs/s/mW.

3.5 Type-0 PPKTP

I now move on to using a Type-0 Periodically Poled Potassium Titanyl-Phosphate (PPKTP) crystal with a poling period of 16.775μm from Raicol with the same setup as before. Type-0 SPDC in PPKTP, unlike the Type-II SPDC for PPLN, makes use of the d_{33} nonlinear coefficient which has a much larger magnitude than the d_{31} nonlinear coefficient of PPLN. The effective nonlinear coefficient d_{eff} has a value of $\approx$12 pm/V[29][24]. Hence I would expect that the output for PPKTP would be at least a $\frac{12^2}{3.4^2} \approx 12$ times brighter than that for PPLN.

3.5.1 Crystal Temperature Tuning

The same procedure for the Type-II PPLN crystal to done to characterise the PPKTP crystal. The same spectrometer is used to obtain the spectrum for the signal and idler from the PPKTP crystal. Based on calculations done using the Sellmeier equations from Emanuali (2003)[18] & Kato (2002)[30], I estimated that the phase matching wavelength is approximately 43°C. Hence, I did a temperature tuning spectrum measurement from a temperature of 35°C to 75°C and the results are plotted on a heatmap as shown in Figure 3.7.

From Figure 3.7, at 43°C, the peak is the highest and hence, I take that as the operating temperature of the PPKTP crystal. With the proper operating temperature, I then optimise the coincidences in the same way that I did for the PPLN crystal by tuning the collection mirrors. A problem that occurred when using this crystal is that the brightness of the output photon pairs were much higher than that for the PPLN crystal and this caused the detectors to saturate and give a lower pair

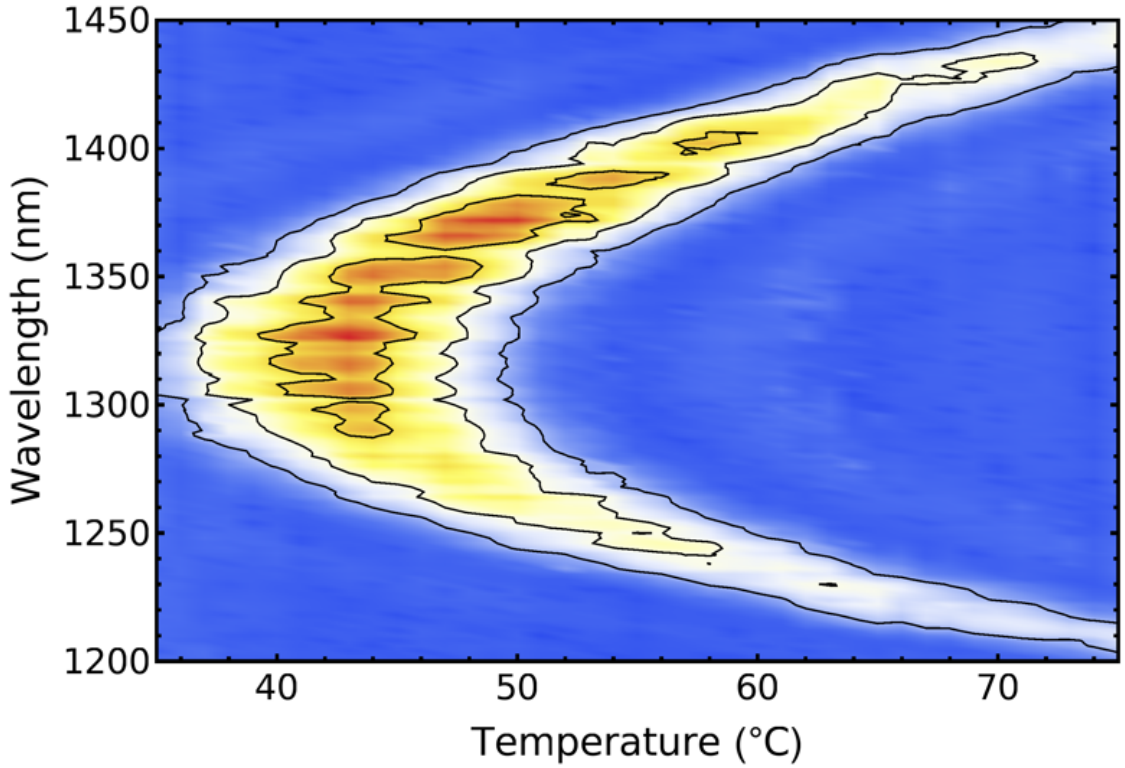

Figure 3.7: Heatmap of SPDC Spectrum for Type-0 PPKTP

rate per mW. To overcome this problem, the pump beam that was coupled into the crystal was slightly misaligned such that the pump power incident on the crystal is lower (≈0.1mW). This caused the singles counts to be within the linear regime of the detectors and a greater pair rate per mW of 57000 pairs/s/mW is observed.

3.6 Comparison of both crystals

From the tests performed as outlined above, I then compare and select the crystal to be used in the correlated photon pair source moving on. The Table 3.2 compares the difference between the two crystals.

Crystal	**Type-II PPLN**	**Type-0 PPKTP**
Output polarisation of photon pairs	$\|H\rangle \rightarrow \|H\rangle\|V\rangle$	$\|V\rangle \rightarrow \|V\rangle\|V\rangle$
Operating Temperature (°C)	23.5	43.0
Highest Pair Rates Observed (/s/mW)	300	57000
Spectrum FWHM of Signal at Operating Temperature (nm)	4	40

Table 3.2: Comparison between Type-II PPLN and Type-0 PPKTP

Comparing the data in the Table 3.2, I then selected the appropriate crystal to use for the source based on the following criteria in descending importance.

- The source has to be bright enough such that I can still detect a reasonable number of photons after ≈25km of fiber.
- The operating temperature of the crystal should be above the room temperature so that it would be easier to stabilise the temperature of the crystal and that the crystal would be above the dew point so there would not be condensation on the crystal.
- The FWHM of the output photons should be as small as possible so that dispersion effects are minimised.

Using this set of criteria, I choose to use the Type-0 PPKTP crystal as the crystal for the final source as it produces the highest coincidence rate and is can be operated at 43°C, which is well above room temperature. The FWHM however, is much higher for the PPKTP crystal compared to the PPLN crystal, but this can be solved by using filters to filter down the output photons FWHM which will be discussed in the following chapters.

Chapter 4

Mitigating the Effects of Chromatic Dispersion

4.1 Chromatic Dispersion & Pulse Broadening

In this chapter, I cover the dispersive effects that optical fibers would have on the signal and idler photons as they propagate through them. The main dispersive effect that would affect the signal and idler photons the most is chromatic dispersion. Chromatic dispersion is the phenomenon where the phase and group velocity of light propagating through a medium depends on the frequency of the light[17].

The reason that chromatic dispersion is a problem is that it causes the output photon pulse to broaden and this would affect the clock synchronisation experiment. The broader pulse would mean that the precision of the clock synchronisation would be lower and dependant on the source which is undesirable. If possible, the source should produce photons with as short pulses as possible such that the limiting factor would be either the jitter time of the detectors or the timing resolution of the time stamping card so that the source can be used with different detectors and time stamping cards without a loss of precision due to the source itself. The jitter time is the distribution of delays between the detection of the photon by the detector and the emission of the electrical signal produced by the detector. The equation governing the dispersive pulse broadening is

$$\tau = \tau_0 \sqrt{1 + (4 \ln 2(\frac{D}{\tau_0^2}))^2} \approx 4 \ln 2(\frac{D}{\tau_0}) \tag{4.1}$$

where τ is the output pulse duration, D is the dispersion parameter, and τ_0 is the

input pulse duration which is dependant on the FWHM of the photons[17].

The dispersion parameter D is given by the equation

$$D \approx \frac{S_0 L}{4}[\lambda - \frac{\lambda_0^4}{\lambda^3}] \tag{4.2}$$

where L is the length of the fiber, S_0 is the zero dispersion slope and λ_0 is the zero dispersion wavelength and their values are 0.086 ps/(nm^2 km) and 1313nm respectively as obtained from the datasheet for a standard Corning SMF-28e Optical fiber.[1]

The FWHM of the photon is related to the pulse duration by the equation

$$\tau = \frac{\lambda^2}{c\Delta\lambda} \tag{4.3}$$

where $\Delta\lambda$ is the FWHM of the photon. From equations 4.1 and 4.2, I can simulate the output pulse duration of the signal and idler photons as they pass through different lengths of fiber for different FWHM of the input signal and idler. The results are shown in the Figures 4.1 and 4.2.

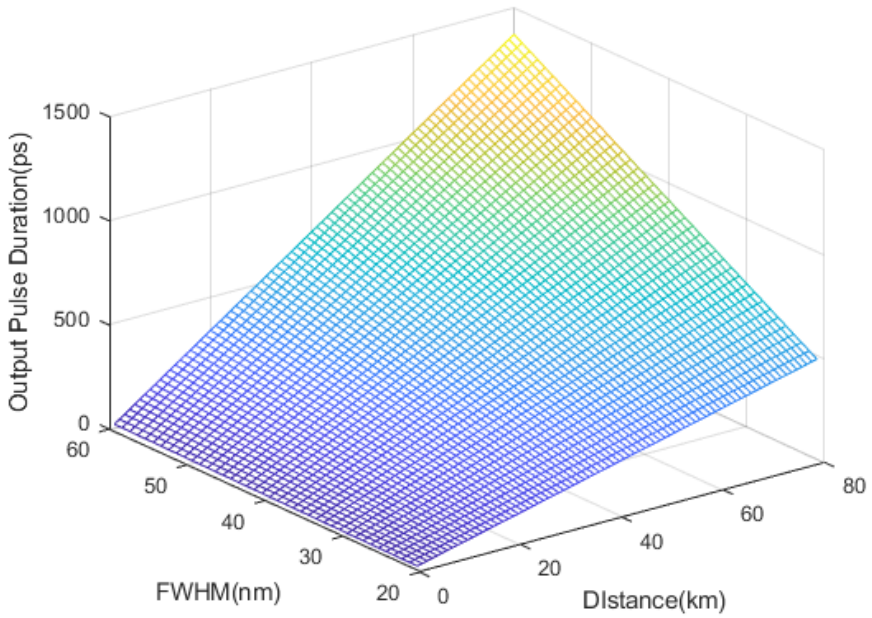

Figure 4.1: Plot of Output Pulse Duration against FWHM & Fiber Length

From the Figures 4.1 and 4.2, as the length of the fiber is increased, the effect on the output pulse duration also increases as expected. Furthermore, the output pulse is also directly dependant on the input signal and idler FWHM.

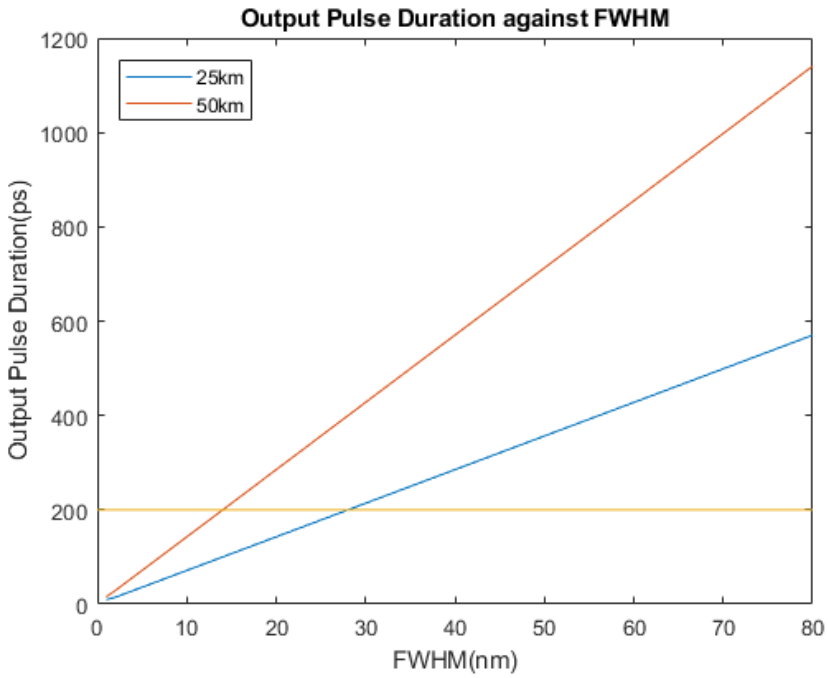

Figure 4.2: Plot of Output Pulse Duration against FWHM of signal for 25km and 50km of Fiber

For this experiment, I would want to have the pulse duration of the photons after they travel through 25km of optical fiber to be smaller than the jitter time of our detectors (ID220). From the datasheet of the ID220 detectors, the jitter time is ≈200ps. Hence, in order to travel through 25km of fiber with an output pulse smaller than 200ps, I would require that the FWHM of the signal and idler photons to be ≈ 20nm. However, as seen in Table 3.2, the FWHM of the signal and idler photons are ≈40nm. Therefore, I would need to filter down the spectrum in order to achieve the FWHM of 20nm.

4.2 Filtering the Signal and Idler

In order to filter the signal and idler, I use a band pass filter (AG Optics) that has a 40nm transmission band centered at 1316nm. This would effectively filter both the signal and idler into a 20nm FWHM. A spectrum of the filtered photons are taken in order to check that the filters are working as intended and is shown in the Figure. From the Figure 4.3, the filters do indeed work as specified and the output spectrum is filtered down to 40nm.

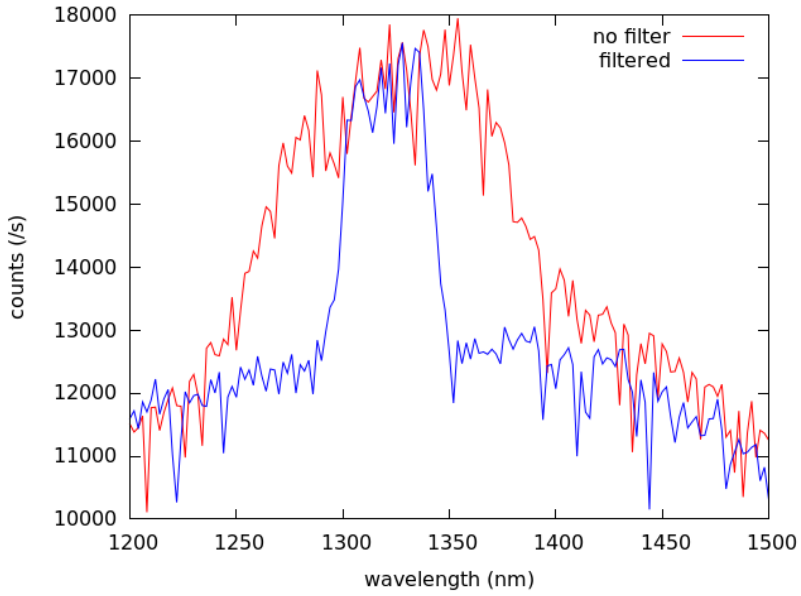

Figure 4.3: Spectrum of output photons with and without Band Pass Filter

I then took another similar spectrum but this time taking the spectrum through each arm of the dichroic fiber beam splitter as well as seen in Figure 4.4.

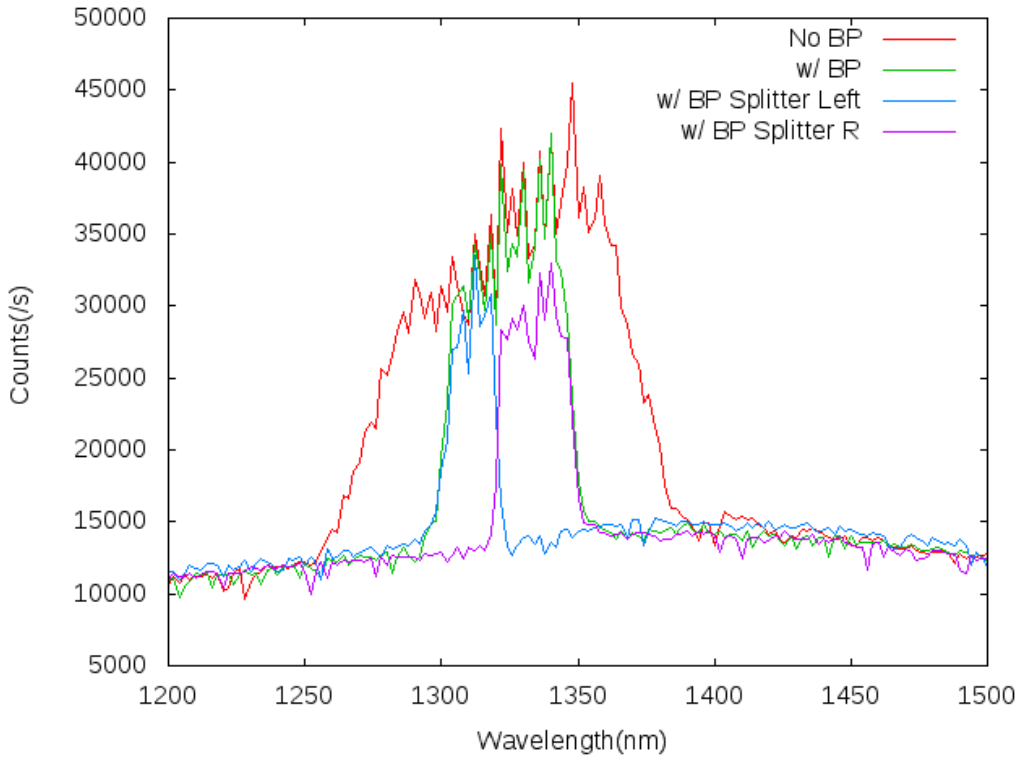

Figure 4.4: Spectrum of the Signal and Idler photons with the Band Pass Filter

A fit to a sinc function is done to the spectrum of each arm to find its FWHM. The left arm has a FWHM of $\approx$ 17nm and the right arm has a FWHM of $\approx$ 25nm. Therefore, I can conclude that the filtering of the spectrum is indeed successful and based on the calculations, the effects of dispersion should be minimised.

4.3 Future Plans

By filtering the signal and idler, I would have theoretically compensated for the chromatic dispersion in the fibers. However, in reality, the dispersion in the fibers may not follow the theoretical calculations exactly and there might be some deviations. In the future, fiber tests are planned in order to test the effects of chromatic dispersion on the photons as well as the attenuation in the fibers. With the results from those tests, I would be able to more accurately compensate for the pulse broadening.

Chapter 5

Designing a Compact Correlated Photon Pair Source

In this chapter, we shall look at the designing and the capabilities of the compact baseplate source.

5.1 Design Considerations

Some of the considerations that should be accounted for in the compact baseplate version of the source are,

- The baseplate source should be small enough such that it can fit into a server rack which has dimensions of 45cm by 45cm.
- The source does not need to have any height restrictions as we can always use more units to house the source.
- The source should be as stable as possible such that minimal adjustments have to be made to ensure optimised coincidence rates.
- The crystal and the pump laser should be temperature stabilised at a temperature above the room temperature.

With these considerations in mind, I then start to devise a prototype for the compact source.

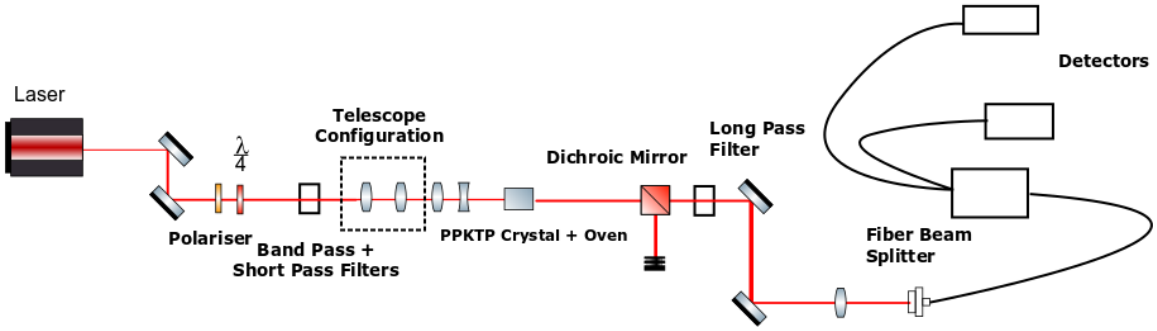

Figure 5.1: Setup of Configuration A

5.2 Compacting the Original Optical Bench Setup

Before starting to design the compact source, I first started to compact the original optical bench source to test the appropriate lenses and distances to use for the compact source.

5.2.1 Configuration A

The first method that I tried to implement was to remove the coupling of the pump laser into a fiber before launching it into the crystal. To do this, I had to modify the setup to accommodate a telescope configuration so that I could more easily adjust the FWHM of the beam at the crystal. Furthermore, I used a concave-convex lens combination to increase the distance between the lenses and the center of the crystal to ensure that there is sufficient space for all the components of the setup. The collection component for this configuration was kept constant.

The Figure 5.1 shows the diagram of the setup of configuration A. As seen in the diagram, we can see that the setup is more compact compared to the initial setup shown in Figure 3.1, as there is no need for the coupling of the pump into a fiber. However, an obvious problem that can be seen is that there is a need to align four lenses, one of which is a concave lens which is very sensitive to small deviations in alignment. This would make the source highly susceptible to temperature fluctuations which may misalign the lenses and mirrors. After building the setup on an optical bench, I then optimised the coincidence rate and managed to obtain a rate of 48000pairs/s/mW, which is slightly lower than that for the initial setup. Another issue with this configuration is that the pairs to singles ratio is much lower compared

to the original setup. This was due to the lack of filtering of the fluorescent photons from the pump because of the removal of the fiber coupling of the pump.

5.2.2 Configuration B

In this configuration, I decided to keep the coupling of the pump into a fiber and shrink the existing setup using different lenses. Using the same method as mentioned in Section 3.3, I tried various lens and distance combination for the pump and collection to obtain the appropriate FWHM. The setup is similar to that shown in Figure 3.1 with the difference being the use of a different lenses and distances to make the source more compact. A detailed diagram of the setup is shown in Figure 5.2.

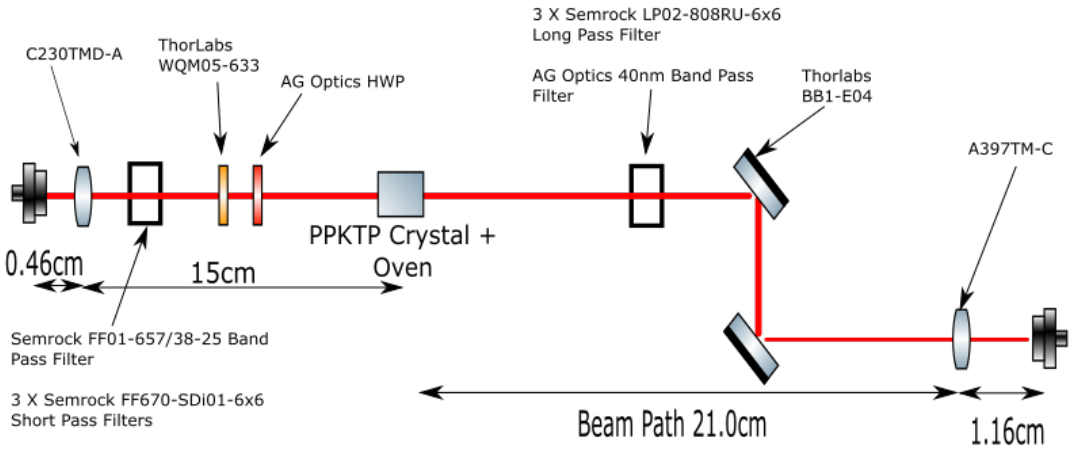

Figure 5.2: Detailed Diagram of Configuration B

With this configuration, the optimised pairs rates observed was 60000 pairs/s/mW, which is slightly better than what was obtained in the original setup. Furthermore, a maximum pair to singles ratio of ≈13% was observed compared to the maximum of 8% seen in the original setup.

5.2.3 Design Choice

Comparing both configurations, configuration B has a higher pair rate and pairs to singles ratio compared to configuration A. The size of A however was much smaller than that of B since there was no need to fiber couple the pump, saving a lot of space. However, there is no need to make the source too small as it only has to eventually

fit into a server rack. Therefore, in order to maximise efficiency, I decided to choose configuration B to base my design on.

5.3 Designing the Baseplate Source

With the chosen design in mind, I then started to design the prototype for the compact baseplate source using Autodesk Inventor. A diagram of the assembly is shown in Figure 5.3.

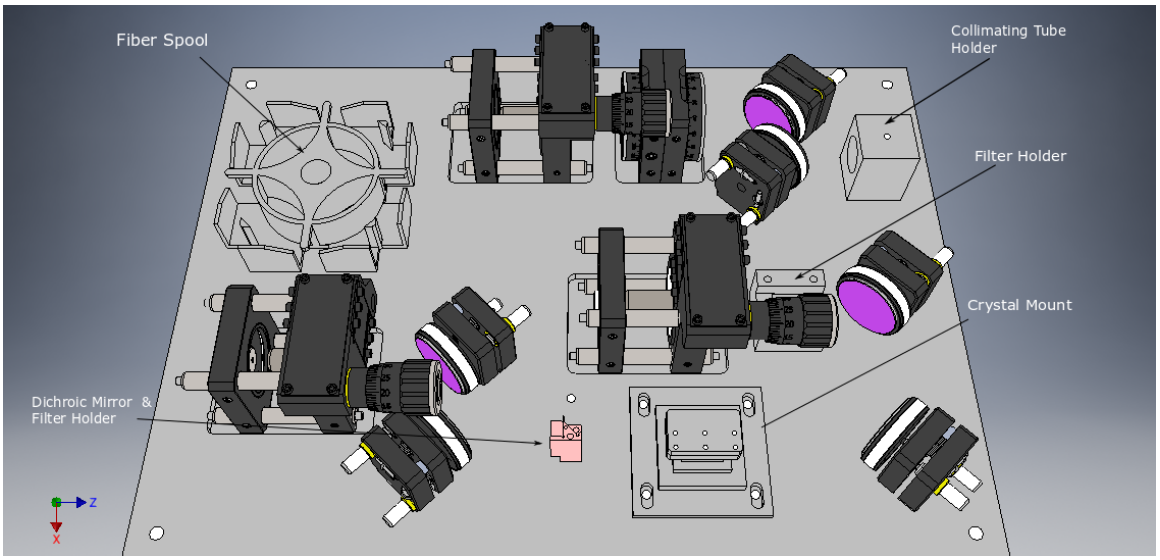

Figure 5.3: Design of Assembled Baseplate Source

The assembly design that I came up with makes use of commercially available Thorlabs mounts for most of the mirrors and lenses. The dimensions of the baseplate are 30cm by 22cm by 1.5cm which are still within the constraints set by the dimensions of a server rack. The only components that had to be designed from scratch were the laser diode collimating tube holder, the filter mounts and the crystal mount.

The design was sent out for fabrication and then assembled. A modification was made to the diode holder to include a TEC on top of the holder in order to temperature stabilise the laser. The pump is aligned through the setup and the signal and idler pairs are then collected. With this current setup, the highest coincidence rate observed were ≈60000 pairs/s/mW which is consistent with what was observed with the bench top source. However, the crystal temperature that gave the optimal pair rates was 28°C which was lower than expected. This was likely due to the fact that a different

laser diode was used and the diode produces a wavelength of 658.3nm compared to 658.8nm. This 0.5nm shift in wavelength according to my simulation, would indeed cause the degenerate phase matching temperature to drop to ≈26°C, which is close to the temperature observed.

In order to rectify this problem, I changed the laser diode to a 660nm laser diode (Ondax SureLock 660nm) which would push the operating temperature up to ≈ 80°C. After optimisation, I managed to observe a maximum coincidence rate of 5200 pairs/s with a pump power of 0.1mW which would give us a rate of ≈52000 pairs/s/mW. With this rate, I then performed a stability test of the source to see if the source continues working stably over a long time. I left the source running overnight for 18 hours and plotted the singles count and the coincidences in the Figure 5.4.

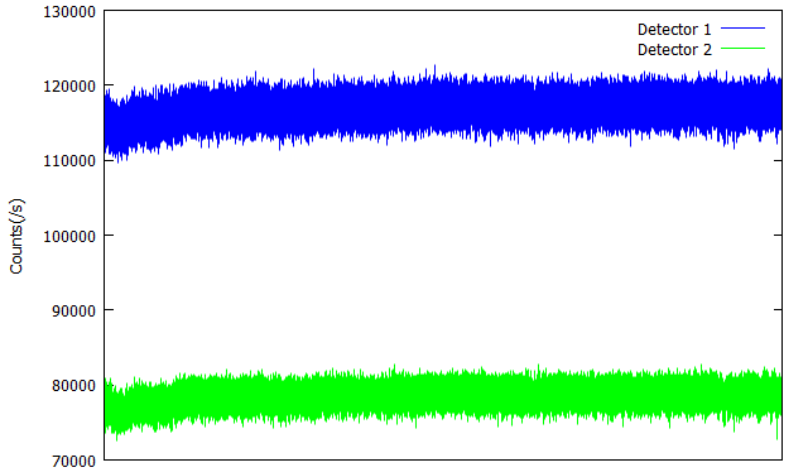

(a) Singles Count for both Detector 1 and 2 over an 18 hour period

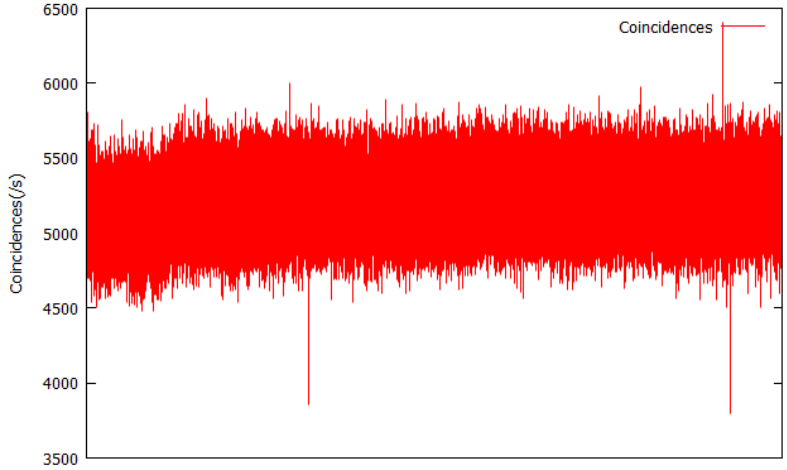

(b) Coincidences over an 18 hour period

Figure 5.4: Stability Test results using 660nm laser diode over an 18 hour period

From the Figure 5.4, it is clear that over the 18 hour period, the source remains working stably and there are no big fluctuations in either the singles or the coincidences. Hence, I can conclude that the source is working stably in the lab. However, since this source is meant to be working in a server rack placed in a room where the temperature might not be constant unlike a lab, I cannot conclude that the source would retain its stability outside the lab environment and further testing have to be done in order to confirm this.

With the data available, I also plotted a histogram of the singles and the coincidences to more accurately determine the mean value of the singles and coincidences. This is shown in Figure 5.5.

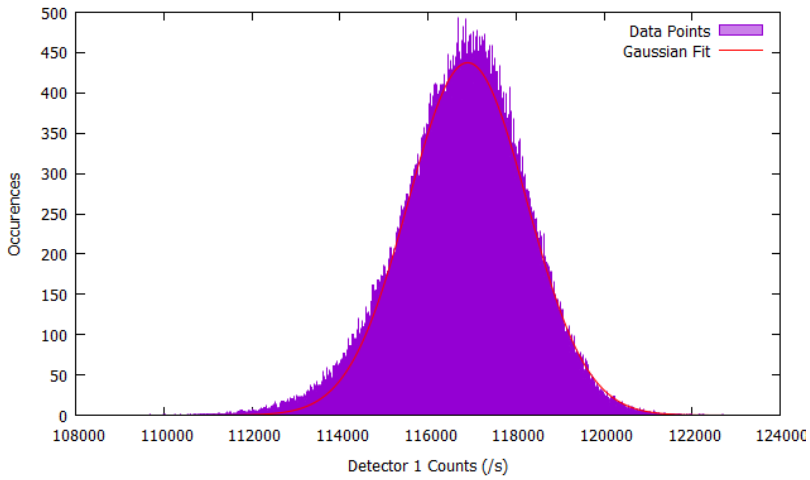

(a) Histogram of Detector 1 Counts and its Gaussian Fit

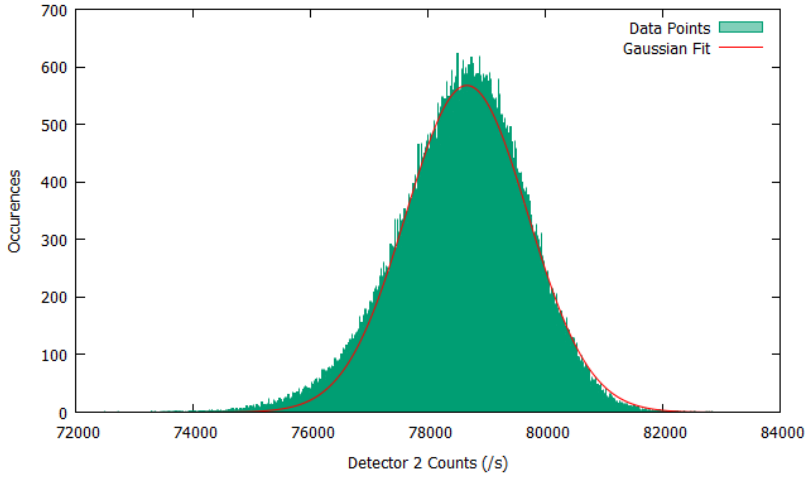

(b) Histogram of Detector 2 Counts and its Gaussian Fit

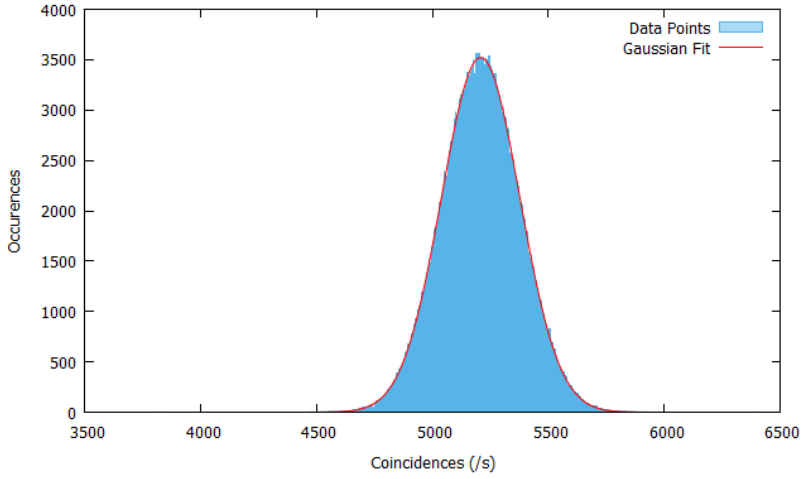

(c) Histogram of Coincidences and its Gaussian Fit

Figure 5.5: Histograms of Singles and Coincidences using data from Stability Test

	Mean	Standard Deviation
Detector 1	116898	1348
Detector 2	78661	1038
Coincidences	5207	169

Table 5.1: Mean and Standard Deviation for the Gaussian fits for Figure 5.5

The table 5.1 shows the mean values of each histogram and its standard deviation. From the table, the mean values for the coincidences are indeed in agreement with my original estimate and the coincidence rate per second per mW is indeed ≈52000 pairs/s/mW. With such high pair rates, the source is now working as intended and can be used for further applications.

Chapter 6

Conclusion & Future Plans

In conclusion, we looked at the testing of two different periodically poled crystals and the building of a correlated photon source. The 2 crystals tested were a Type-II PPLN crystal and a Type-0 PPKTP crystal. The crystal chosen for the rest of the project was the Type-0 PPKTP which showed a much higher brightness than the PPLN crystal.

We then looked at the effects of chromatic dispersion in optical fibers in order to compensate for their impact on the signal and idler photons. The pulse broadening due to chromatic dispersion was simulated and measures to reduce this effect was tested. A 40nm band pass filter was used in order to filter down the signal and idler into a FWHM of 20nm in order to reduce the broadening effect.

Finally, we looked at designing and testing different configurations for the portable baseplate source. After selecting the configuration B due to higher efficiency, I then built the source and tested its capabilities. The source is now currently able to produce correlated photon pairs at a rate of 52000pairs/s/mW which is sufficient for currently planned deployment.

Looking forwards, now with a working portable source, we are now able to use it to test various effects such as the chromatic dispersion in buried fibers around the country. Furthermore, we can now move on to perform the clock synchronisation experiment which is outlined by Ho et al.[5] to further test the capability of the correlated photon source in a real world application.

Appendix A

Gaussian Beam Parameter Calculation

In this appendix, we shall look into the calculations involved in estimating the FWHM of a gaussian beam using an ABCD matrix. A gaussian beam can be expressed as a complex q parameter given by

$$\frac{1}{q} = -i\frac{\lambda}{\pi w^2} + \frac{1}{R} \tag{A.1}$$

where λ is the wavelength of the beam, w is the beam radius, and R is the radius of curvature of the beam.

The q parameter transforms as the gaussian beam propagates through an optical media. The new q' parameter is given by

$$q' = \frac{Aq + B}{Cq + D} \tag{A.2}$$

where the values of A, B, C, and D come from the associated ABCD matrix of the optical media.

Some common ABCD matrices are,

Optical media	ABCD matrix
Free Space	$\begin{pmatrix} 1 & d \\ 0 & 1 \end{pmatrix}$
Medium with refractive index n	$\begin{pmatrix} 1 & nd \\ 0 & n \end{pmatrix}$
Thin Lens of focal length f	$\begin{pmatrix} 1 & 0 \\ -\frac{1}{f} & 1 \end{pmatrix}$

Table A.1: Commonly used ABCD matrices[3]

Using these matrices, the new q parameter can be determined through matrix multiplication of the appropriate ABCD matrix and applying it to the initial q parameter. For the setup in Chapter 3, the overall ABCD matrix is

$$\begin{pmatrix} A & B \\ C & D \end{pmatrix} = \begin{pmatrix} 1 & d_2 \\ 0 & 1 \end{pmatrix} \begin{pmatrix} 1 & 0 \\ -\frac{1}{f} & 1 \end{pmatrix} \begin{pmatrix} 1 & d_1 \\ 0 & 1 \end{pmatrix} \tag{A.3}$$

where d_1 is the distance from the initial position to the lens, f is the focal length of the lens and d_2 is the distance from the lens to the center of the crystal.

With the matrix calculated, the new complex parameter q' can be calculated from the initial q. From q', I would then be able to obtain the beam radius at the crystal center. The radius can then be converted into FWHM using the relation

$$FWHM = 1.18w \tag{A.4}$$

References

[1] Corning Inc. *Corning SMF-28e Optical Fiber Product Information*, January 2005.

[2] Robert W. Boyd. Chapter 2 - wave-equation description of nonlinear optical interactions. In Robert W. Boyd, editor, *Nonlinear Optics (Third Edition)*, pages 69 – 133. Academic Press, Burlington, third edition edition, 2008.

[3] Justin Peatross and Michael Ware. Physics of light and optics: A free online textbook. In *Frontiers in Optics 2010/Laser Science XXVI*, page JWA64. Optical Society of America, 2010.

[4] Roy J. Glauber. Nobel lecture: One hundred years of light quanta. *Reviews of Modern Physics*, 78(4):1267–1278, 2006.

[5] Caleb Ho, AntÃŋa Lamas-Linares, and Christian Kurtsiefer. Clock synchronization by remote detection of correlated photon pairs. *New Journal of Physics*, 11(4):045011, 2009.

[6] Xiongfeng Ma, Chi-Hang Fred Fung, and Hoi-Kwong Lo. Quantum key distribution with entangled photon sources. *Phys. Rev. A*, 76:012307, Jul 2007.

[7] ALEXANDER LING EUK JIN. *Entangled state preparation for optical quantum communication: Creating and characterizing photon pairs from Spontaneous Parametric Down Conversion inside bulk uniaxial crystals*. PhD thesis, 2008.

[8] SIDDARTH K. JOSHI. *Entangled Photon Pairs: Efficient Generation and Detection, and Bit Commitment*. PhD thesis, 2014.

[9] Charles H. Bennett and Gilles Brassard. Quantum cryptography: Public key distribution and coin tossing. *Theoretical Computer Science*, 560:7–11, 2014.

[10] Artur K. Ekert. Quantum cryptography based on bellâĂŹs theorem. *Physical Review Letters*, 67(6):661–663, 1991.

[11] Robert Bedington, Juan M. Arrazola, and Alexander Ling. Progress in satellite quantum key distribution. *NPJ Quantum Information*, 3:1, 2017.

[12] Sheng-Kai Liao, Wen-Qi Cai, Wei-Yue Liu, Liang Zhang, Yang Li, Ji-Gang Ren, Juan Yin, Qi Shen, Yuan Cao, Zheng-Ping Li, Feng-Zhi Li, Xia-Wei Chen, Li-Hua Sun, Jian-Jun Jia, Jin-Cai Wu, Xiao-Jun Jiang, Jian-Feng Wang, Yong-Mei Huang, Qiang Wang, Yi-Lin Zhou, Lei Deng, Tao Xi, Lu Ma, Tai Hu, Qiang Zhang, Yu-Ao Chen, Nai-Le Liu, Xiang-Bin Wang, Zhen-Cai Zhu, Chao-Yang Lu, Rong Shu, Cheng-Zhi Peng, Jian-Yu Wang, and Jian-Wei Pan. Satellite-to-ground quantum key distribution. *Nature*, 549(7670):43, 2017.

[13] Alessandro Restelli, Joshua C Bienfang, and Alan L Migdall. Single-photon detection efficiency up to 50% at 1310 nm with an ingaas/inp avalanche diode gated at 1.25 ghz. *Applied Physics Letters*, 102(14):141104, 2013.

[14] Robert W. Boyd. Chapter 1 - the nonlinear optical susceptibility. In Robert W. Boyd, editor, *Nonlinear Optics (Third Edition)*, pages 1 – 67. Academic Press, Burlington, third edition edition, 2008.

[15] Pavel Trojek. Efficient generation of photonic entanglement and multiparty quantum communication. December 2007.

[16] G.G.Gurzadien, V.G.Dmitriev, and D.N.Nikogosian. *Handbook of nonlinear optical crystals*, volume 64.;64;. Springer, New York;Berlin;, 3rd, rev. edition, 1999.

[17] Rüdiger Paschotta. *Encyclopedia of laser physics and technology.* Wiley-VCH, Chichester;Weinheim;, 2008.

[18] Shai Emanueli and Ady Arie. Temperature-dependent dispersion equations for ktiopo4 and ktioaso4. *Appl. Opt.*, 42(33):6661–6665, Nov 2003.

[19] Chun-Yao Yang, Chun Lin, Charlotte Liljestrand, Wei-Min Su, Carlota Canalias, Chih-Sung Chuu, Skolan fÃűr teknikvetenskap (SCI), TillÃďmpad fysik, KTH, and Laserfysik. Parametric down-conversion with nonideal and random quasi-phase-matching. *Scientific reports*, 6:26079, 2016.

[20] M. M. Fejer, G. A. Magel, D. H. Jundt, and R. L. Byer. Quasi-phase-matched second harmonic generation: tuning and tolerances. *IEEE Journal of Quantum Electronics*, 28(11):2631–2654, 1992.

[21] J. A. Armstrong, N. Bloembergen, J. Ducuing, and P. S. Pershan. Interactions between light waves in a nonlinear dielectric. *Phys. Rev.*, 127:1918–1939, Sep 1962.

[22] P. A. Franken and J. F. Ward. Optical harmonics and nonlinear phenomena. *Rev. Mod. Phys.*, 35:23–39, Jan 1963.

[23] David S. Hum and Martin M. Fejer. Quasi-phasematching. *Comptes rendus - Physique*, 8(2):180–198, 2007.

[24] Fabian Steinlechner, Pavel Trojek, Marc Jofre, Henning Weier, Daniel Perez, Thomas Jennewein, Rupert Ursin, John Rarity, Morgan W. Mitchell, Juan P. Torres, Harald Weinfurter, and Valerio Pruneri. A high-brightness source of polarization-entangled photons optimized for applications in free space. *Optics express*, 20(9):9640, 2012.

[25] Ryan S. Bennink. Optimal collinear gaussian beams for spontaneous parametric down-conversion. *Phys. Rev. A*, 81:053805, May 2010.

[26] P. B. Dixon, Danna Rosenberg, Veronika Stelmakh, Matthew E. Grein, Ryan S. Bennink, Eric A. Dauler, Andrew J. Kerman, Richard J. Molnar, and Franco N. C. Wong. Heralding efficiency and correlated-mode coupling of near-ir fiber-coupled photon pairs. *Physical Review A*, 90(4), 2014.

[27] Olivier Alibart, Virginia D 'auria, Marc De Micheli, Florent Doutre, Florian Kaiser, Laurent LabontÃľ, Tommaso Lunghi, Eric Picholle, and SÃľbastien Tanzilli. Quantum photonics at telecom wavelengths based on lithium niobate waveguides. *Journal of Optics*, 18(10):104001, 2016.

[28] Covesion guide to ppln - material properties of lithium niobate. Available at `https://www.covesion.com/support/covesion-guide-to-ppln/material-properties-of-lithium-niobate.html`(2018/04/02).

[29] S. Chaitanya Kumar, G. K. Samanta, and M. Ebrahim-Zadeh. High-power, single-frequency, continuous-wave second-harmonic-generation of ytterbium fiber laser in ppktp and mgo:spplt. *Opt. Express*, 17(16):13711–13726, Aug 2009.

[30] Kiyoshi Kato and Eiko Takaoka. Sellmeier and thermo-optic dispersion formulas for ktp. *Appl. Opt.*, 41(24):5040–5044, Aug 2002.